Quantum Electronics **39** (9) 814 – 820 (2009)

ACTIVE MEDIA

PACS numbers: 42.55.Rz; 42.60.Jf
DOI: 10.1070/QE2009v039n09ABEH014039

Nonlinear thermally induced distortions of a laser beam in a cryogenic disk amplifier

A.G. Vyatkin, E.A. Khazanov

Abstract. **Taking into account the temperature dependences of the heat conductivity, the refractive index, and the thermal expansion coefficient, we calculated the temperature, elastic stresses, a thermally induced lens and depolarisation of a beam in a cryogenic disk amplifier (an Yb : YAG disk placed between a copper cylinder and a sapphire disk cooled by liquid nitrogen). When the active element (the thickness is 0.6 mm, the orientation is [001], the atomic concentration of Yb is 10 %) is pumped by radiation from a diode laser (the beam diameter is 6 mm), the temperature does not exceed 140 K for the heat release power of 100 W. In this case, elastic stresses in the active element are six times lower than the maximum permissible value. The focal distance of the thermally induced lens is 5.5 m and the depolarisation rate is 0.038 % per two passes through the active element. Although the heat conductivity of the active element rapidly decreases with temperature, the thermal load can be increased by 1.5 – 2 times when the dimensions of the active element remain constant.**

Keywords: *cryogenic disk laser, nonlinear heat conduction equation, thermal lens, depolarisation, photoelastic effect, method of finite elements.*

1. Introduction

At present, solid-state lasers with high peak and average powers and the close-to-diffraction beam quality are being actively developed all over the world. A rapid increase in the output power of solid-state lasers became possible due to a wide spread of diode pumping, application of active ions with a small quantum defect, and the development of fabrication technologies of optical materials.

In designing high-average-power lasers, one of the main problems is parasitic thermal effects in optical elements. They include the increase in the volume-averaged temperature, thermally induced elastic stresses, phase and polarisation distortions of the beam [1, 2]. In elements made of laser ceramics, these effects also involve a thermally induced small-scale spatial modulation of the beam polarisation and phase [3, 4]. The increase in the average temperature of the active element leads, as a rule, to an undesirable change in its physical properties: a decrease in the heat conductivity, an increase in the thermal expansion coefficient and the thermooptic coefficient, a decrease in the stimulated emission cross section at the lasing transition, etc. On the contrary, cooling atoms down to liquid nitrogen temperatures allows one to improve significantly the properties of the medium [5, 6]. However, at a large heat release, the temperature substantially exceeds 77 K and the heat conduction problem becomes nonlinear.

The temperature gradient in the active element leads to the appearance of elastic stresses. When they exceed some limiting value, the sample is damaged [7]. The decrease in the thermal expansion coefficient during cooling results in a decrease in the elastic stresses and phase distortions. The latter appear due to a change in the sample length resulting from the thermal expansion, temperature dependence of the refractive index and the photoelastic effect [1, 8]. The photoelastic effect also causes a change in the polarisation of radiation propagating through the medium.

Heat release in the active element of a solid-state laser is associated with the quantum defect as well as the absorption of laser radiation by ions in the excited state, up conversion and cross relaxation [9]. To reduce the heat release, it is necessary to select active ions with a small quantum defect where the mentioned parasitic processes are absent. One of the best candidates is the Yb^{3+} ion [10]. As an active element matrix it is desirable to use a substance with a high heat conductivity and resistance. For Yb^{3+} ions, the suitable matrix is the YAG crystal.

To decrease the temperature and its gradient, active elements having a special geometry with a large surface area through which heat is released, are actively used. The example is a thin end-pumped disk, end coupling in/coupling out of radiation and end-face cooling with the help of heatsinks made of materials with a high heat conductivity [11, 12]. It was noted in [13] that the proximity of atomic radii of Yb and Y makes it possible to fabricate active Yb : YAG elements with a high doping level (atomic concentration is tens of percents), which allows one to avoid multipass schemes while designing thin disk lasers.

This work is devoted to the study of thermally induced distortions in a disk Yb : YAG laser amplifier cooled by liquid nitrogen. We solved the nonlinear stationary problem of heat conduction for a system consisting of an active disk and heatsinks, the stationary elasticity problem for an active disk, and calculated the thermally induced distortions of the laser beam.

A.G. Vyatkin, E.A. Khazanov Institute of Applied Physics, Russian Academy of Sciences, ul. Ul'yanova 46, 603950 Nizhnii Novgorod, Russia; e-mail: vyatkin@appl.sci-nov.ru, khazanov@appl.sci-nnov.ru

Received 26 December 2008
Kvantovaya Elektronika **39** (9) 814 – 820 (2009)
Translated by I.A. Ulitkin

2. Solution of the heat conduction problem

First of all, it is necessary to find the temperature distribution in a system consisting of three coaxial cylindrical bodies: active Yb : YAG element placed between two heatsinks (Fig. 1) – a copper cylinder and a disk made of an optically transparent material. The disk can be manufactured, for example, from sapphire, diamond or undoped YAG (below, we will call it a sapphire disk).

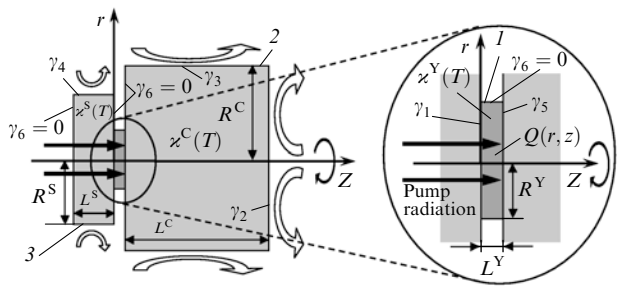

Figure 1. Scheme of cooling active element (*1*) with the help of copper (*2*) and sapphire (*3*) heatsinks. White arrows show cooling by liquid nitrogen; $\varkappa^{\mathrm{Y}}$, $\varkappa^{\mathrm{C}}$, and $\varkappa^{\mathrm{S}}$ are the heat conductivitys of Yb : YAG, copper, and sapphire, respectively; $\gamma_1 - \gamma_6$ are the coefficients of the heat transfer through the corresponding surfaces.

We will assume, unless otherwise specified, that the coordinate axis z is local for each of three bodies in the system (the axes are directed from left to right, the origins of the coordinates coincide with the left end faces of these bodies) and the Z axis – global and coincides with the z axis of the active element.

2.1 General formulation of the heat conduction problem

Let an axially symmetric pump beam with the spatial profile $f(r)$ be incident on the system from the side of the sapphire disk. Radiation is absorbed in the active element during its propagation, reflected from the mirror coated on the crystal, and propagates through the disk in the backward direction, thus experiencing further absorption, and then is coupled out from the system. By assuming absorption in the medium to be independent of the temperature and radiation intensity and the heat release power to be proportional to the absorbed power, we obtain the density of the heat release power in the active element

$$Q(r,z) = Q_0 f(r) g(z),$$
$$g(z) = \exp(-\alpha_{\mathrm{abs}} z) + \exp\left[\alpha_{\mathrm{abs}}\left(z - 2L^{\mathrm{Y}}\right)\right], \tag{1}$$

where α_{abs} is the coefficient of linear radiation absorption by the medium; L^{Y} is the active element thickness; Q_0 is the proportionality coefficient.

We will assume for simplicity that both heatsinks are cooled directly and axially symmetric by liquid nitrogen, the anisotropy of the thermal conductivity tensor of sapphire being neglected. Within the framework of simplifying assumptions, the heat conduction problem becomes axially symmetric.

Analytic approximation of the temperature dependence of the YAG heat conductivity was borrowed from paper [6]. However, the heat conductivity depends on the dopant concentration, which is substantial for highly doped active elements (tens of percent). The dependence of the Yb : YAG heat conductivity on the atomic concentration of active ions at room temperature is presented in paper [13]. Because the data on the temperature dependence of the heat conductivity of doped Yb : YAG crystals is insufficient, it was suggested that doping decreases thermal conductivity to the same extent in the entire temperature region of interest (77 K – 350 K).

The stationary heat conduction equation has the from

$$\mathrm{div}[\varkappa(T)\nabla T] + Q(\boldsymbol{r}) = 0, \tag{2}$$

where T is the temperature; $\varkappa(T)$ is the heat conductivity. We will write the boundary conditions in the form

$$\varkappa(T)\left.\frac{\partial T}{\partial n}\right|_{\Gamma} = \gamma(T_{\mathrm{ext}} - T)|_{\Gamma}, \tag{3}$$

where Γ is the boundary surface (the derivative of the temperature is taken along the direction of the external normal $\boldsymbol{n}$ to it); γ is the coefficient of the heat transfer through the surface of the thermal contact; T_{ext} is the temperature of the body in contact with this along the surface Γ.

A plastic thermal interface is usually present on the surfaces of the thermal contact between the active element and the heatsinks. By filling the gaps between the bodies, it improves the heat transfer through the contact, i.e. increases γ. Thus, an indium film or thermal grease is applied on the boundary with copper. The efficiencies of different thermal interfaces are compared in paper [14].

In the linear approximation, system (2), (3) allows the analytic solution, which will be discussed in section 2.2. In the nonlinear case, only the numerical solution presented in section 2.3 is possible.

2.2 Analytic solution of the heat conduction problem

To solve analytically the heat conduction problem, we will use the method of Green's functions. For a cylindrical body ($0 \leqslant r \leqslant R$, $0 \leqslant z \leqslant L$), the solution of the Poisson equation [equation (2) at $\varkappa = \mathrm{const}$] with inhomogeneous boundary conditions of the third kind (3) at any point can be represented as a sum of integrals in volume and surface sources. The coolant temperature will be assumed the same for both heatsinks and independent of the coordinates. In this case, due to the linearity of the problem, the temperature can be measured from the coolant temperature and the latter can be added to the solution at the final stage. Then, the expressions for temperatures of the bodies in the system can be written in the form [15]

$$T^{\mathrm{Y}}(r,z) = \sum_{m,s} \frac{J_0\left(\tilde{\mu}_m^{\mathrm{Y}} r\right)}{N_{ms}^{\mathrm{Y}}} \frac{h_s^{\mathrm{Y}}(z)}{} \Bigg[f_{11} F_m G_s + \bar{\lambda}_1^{\mathrm{C}} h_s^{\mathrm{Y}}(L^{\mathrm{Y}}) \int_0^{R^{\mathrm{Y}}} J_0\left(\tilde{\mu}_m^{\mathrm{Y}} \xi\right) T^{\mathrm{C}}(\xi, 0)\, \xi \mathrm{d}\xi + \bar{\lambda}_1^{\mathrm{S}} h_s^{\mathrm{Y}}(0) \int_0^{R^{\mathrm{Y}}} J_0\left(\tilde{\mu}_m^{\mathrm{Y}} \xi\right) T^{\mathrm{S}}(\xi, L^{\mathrm{S}})\, \xi \mathrm{d}\xi \Bigg],$$

$$T^{\mathrm{C}}(r,z)=\sum_{m,s}\frac{J_0\left(\tilde{\mu}_m^{\mathrm{C}}r\right)}{N_{ms}^{\mathrm{C}}}\frac{h_s^{\mathrm{C}}(z)}{\bar{\lambda}_2^{\mathrm{C}}h_s^{\mathrm{C}}(0)}$$
$$\times\left[\int_0^{R^{\mathrm{Y}}}J_0\left(\tilde{\mu}_m^{\mathrm{C}}\xi\right)T^{\mathrm{Y}}(\xi,L^{\mathrm{Y}})\xi\mathrm{d}\xi+\int_{R^{\mathrm{Y}}}^{R^{\mathrm{C}}}J_0\left(\tilde{\mu}_m^{\mathrm{C}}\xi\right)T^{\mathrm{C}}(\xi,0)\xi\mathrm{d}\xi\right], \tag{4}$$

$$T^{\mathrm{S}}(r,z)=\sum_{m,s}\frac{J_0\left(\tilde{\mu}_m^{\mathrm{S}}r\right)}{N_{ms}^{\mathrm{S}}}\frac{h_s^{\mathrm{S}}(z)}{\bar{\lambda}_2^{\mathrm{S}}h_s^{\mathrm{S}}(L^{\mathrm{S}})}$$
$$\times\left[\int_0^{R^{\mathrm{Y}}}J_0\left(\tilde{\mu}_m^{\mathrm{S}}\xi\right)T^{\mathrm{Y}}(\xi,0)\xi\mathrm{d}\xi+\int_{R^{\mathrm{Y}}}^{R^{\mathrm{S}}}J_0\left(\tilde{\mu}_m^{\mathrm{S}}\xi\right)T^{\mathrm{S}}(\xi,L^{\mathrm{S}})\xi\mathrm{d}\xi\right],$$

where J_0 and J_1 are the zero- and first-order Bessel functions of the first kind; the superscripts Y, C, and S denote the belonging of the quantity to the active element, copper, and sapphire, respectively;

$$\bar{\lambda}_1^{\mathrm{C}}=\frac{2\pi\gamma_5}{\varkappa^{\mathrm{Y}}};\ \bar{\lambda}_1^{\mathrm{S}}=\frac{2\pi\gamma_1}{\varkappa^{\mathrm{Y}}};\ \bar{\lambda}_2^{\mathrm{C}}=\frac{2\pi\gamma_5}{\varkappa^{\mathrm{C}}};\ \bar{\lambda}_2^{\mathrm{S}}=\frac{2\pi\gamma_1}{\varkappa^{\mathrm{S}}};\ f_{11}=\frac{2\pi Q_0}{\varkappa^{\mathrm{Y}}};$$
$$F_m=\int_0^{R^{\mathrm{Y}}}J_0\left(\tilde{\mu}_m^{\mathrm{Y}}\xi\right)f(\xi)\xi\mathrm{d}\xi;\ G_s=\int_0^{L^{\mathrm{Y}}}h_s^{\mathrm{Y}}(\zeta)g(\zeta)\mathrm{d}\zeta; \tag{5}$$

$$N_{ms}=\frac{\pi R^2}{2}\left[J_0^2(\tilde{\mu}_mR)+J_1^2(\tilde{\mu}_mR)\right]\left(1+\frac{\tilde{\mu}_m^2}{\lambda_s^2}\right)$$
$$\times\left[\left(\lambda_s^2+k_2^2\right)\left(\frac{k_3}{\lambda_s^2+k_3^2}+L\right)+k_2\right]; \tag{6}$$

$$h_s(z)=\cos(\lambda_sz)+\frac{k_2}{\lambda_s}\sin(\lambda_sz); \tag{7}$$

$\tilde{\mu}_m$ and λ_s are nonnegative roots of transcendental equations

$$\tilde{\mu}_mJ_1(\tilde{\mu}_mR)=k_1J_0(\tilde{\mu}_mR),\quad\frac{\tan(\lambda_sL)}{\lambda_s}=\frac{k_2+k_3}{\lambda_s^2-k_2k_3}; \tag{8}$$

$$\{k_1,k_2,k_3,L,R\}$$
$$=\begin{cases}\{0,\gamma_1/\varkappa^{\mathrm{Y}},\gamma_5/\varkappa^{\mathrm{Y}},L^{\mathrm{Y}},R^{\mathrm{Y}}\}\text{ for YAG}:\mathrm{Yb},\\ \{\gamma_3/\varkappa^{\mathrm{C}},\gamma_5/\varkappa^{\mathrm{C}},\gamma_2/\varkappa^{\mathrm{C}},L^{\mathrm{C}},R^{\mathrm{C}}\}\text{ for copper},\\ \{\gamma_4/\varkappa^{\mathrm{S}},0,\gamma_1/\varkappa^{\mathrm{S}},L^{\mathrm{S}},R^{\mathrm{S}}\text{ for sapphire}.\end{cases} \tag{9}$$

The summation indices m and s in (4) change, strictly speaking, from 1 to ∞, but in practical calculations it is necessary to leave a finite number of terms in all the series. Let us explain the meaning of underlying the set of multipliers in (4). The method of Green's functions does not allow one to find a reliable solution at the interfaces of bodies with an inhomogeneous boundary condition, i.e. at those interfaces where the thermal contact between the bodies takes place. The behaviour of the solution mainly resembles that of the Fourier series near the point of the discontinuity of the first kind. Because of truncation of series in (4), the solution is incorrect in the region with the dimension of the order of the oscillation period of the first neglected term and in the rest of the body it acquires an undesirable modulation. In the theory of Fourier series this effect is called the Gibbs phenomenon. Because the acquiring of the reliable solution plays an important role for solving the problem of the thermal contact between the bodies, these artefacts should be eliminated.

Solution (4) was corrected by using the following algorithm. First, to eliminate the Gibbs phenomenon, we used the N_{L}-fold ($N_{\mathrm{L}}\simeq 2-3$) Lanczos smoothing [16] along the coordinate axes r and z. Second, the solution in the near-boundary region was obtained with the help of the polynomial extrapolation by the least squares method of the solution in the region more remote from the boundary, which after smoothing can be assumed valid. We can show that these procedures do not change the scheme of the solution and only lead to transformation of the functions underlined in (4):

$$\underline{J_0(\tilde{\mu}_mr)}=\tilde{l}_m^{N_{\mathrm{L}}}J_0(\tilde{\mu}_mr),$$

$$\underline{h_s(z)}=l_s^{N_{\mathrm{L}}}\left[K_s^{(0N)}h_s(\Delta)+\sum_{j=1}^{N}K_s^{(jN)}\frac{1}{j!}\left(\frac{z-\Delta}{\delta}\right)^j\right.$$
$$\left.\times\frac{1}{\lambda_s^j}\left.\frac{\mathrm{d}^jh_s(\zeta)}{\mathrm{d}\zeta^j}\right|_{\zeta=\Delta}\right]\text{ at }0\leqslant z<\Delta,$$

$$\underline{h_s(z)}=l_s^{N_{\mathrm{L}}}h_s(z)\text{ at }\Delta\leqslant z\leqslant L-\Delta, \tag{10}$$

$$\underline{h_s(z)}=l_s^{N_{\mathrm{L}}}\left[K_s^{(0N)}h_s(L-\Delta)+\sum_{j=1}^{N}K_s^{(jN)}\frac{1}{j!}\left(\frac{\Delta+z-L}{\delta}\right)^j\right.$$
$$\left.\times\frac{1}{\lambda_s^j}\left.\frac{\mathrm{d}^jh_s(\zeta)}{\mathrm{d}\zeta^j}\right|_{\zeta=L-\Delta}\right]\text{ at }L-\Delta<z\leqslant L.$$

Here, δ is the half-period of the first neglected harmonic in the series with respect to s in (4); Δ is the distance equal to two–three periods of the same harmonic; $N\simeq 1-3$ is the major degree of the extrapolating polynomial fitted experimentally; in the case of extrapolation by the linear function, which proved the most efficient, the coefficients

$$K_s^{(01)}=l_s,\quad K_s^{(11)}=3\,\frac{l_s-\cos(\lambda_s\delta)}{\lambda_s\delta}; \tag{11}$$

$$\tilde{l}_m=\frac{\sin(\tilde{\mu}_m\tilde{\delta})}{\tilde{\mu}_m\tilde{\delta}},\quad l_s=\frac{\sin(\lambda_s\delta)}{\lambda_s\delta} \tag{12}$$

are the smoothing Lanczos factors along the r and z axes, respectively; $\tilde{\delta}$ is half the quasi-period of the first neglected term in the series with respect to m in (4).

By using expression (4), for temperatures at $Z=0$ and $Z=L^{\mathrm{Y}}$ we can write the closed system of equations

$$\hat{\Theta}(r)=\int_0^{R_{\max}}\sum_m\hat{\Phi}_m(r)\hat{\Psi}_m(\xi)\hat{\Theta}(\xi)\xi\mathrm{d}\xi+\hat{f}(r), \tag{13}$$

where

$$\hat{\Theta}(r)=\begin{pmatrix}T^{\mathrm{S}}(r,L^{\mathrm{S}})\\ T^{\mathrm{Y}}(r,0)\\ T^{\mathrm{Y}}(r,L^{\mathrm{Y}})\\ T^{\mathrm{C}}(r,0)\end{pmatrix};\quad\hat{f}(r)=f_{11}\begin{pmatrix}0\\ \sum_m\underline{J_0\left(\tilde{\mu}_m^{\mathrm{Y}}r\right)}\tilde{Q}_m^{(0)}\\ \sum_m\underline{J_0\left(\tilde{\mu}_m^{\mathrm{Y}}r\right)}\tilde{Q}_m^{(1)}\\ 0\end{pmatrix};$$

$$\hat{\Phi}_m(r) = \begin{pmatrix} \underline{J_0(\tilde{\mu}_m^{\mathrm{S}} r)} & 0 & 0 & 0 \\ 0 & \underline{J_0(\tilde{\mu}_m^{\mathrm{Y}} r)} & 0 & 0 \\ 0 & 0 & \underline{J_0(\tilde{\mu}_m^{\mathrm{Y}} r)} & 0 \\ 0 & 0 & 0 & \underline{J_0(\tilde{\mu}_m^{\mathrm{C}} r)} \end{pmatrix}; \quad (14)$$

$$\hat{\Psi}_m(r) = \begin{pmatrix} \bar{\lambda}_2^{\mathrm{S}} \tilde{R}_m^{\mathrm{S}} \hat{1}_{[R^{\mathrm{Y}}, R^{\mathrm{S}}]}(r) J_0(\tilde{\mu}_m^{\mathrm{S}} r) & \bar{\lambda}_2^{\mathrm{S}} \tilde{R}_m^{\mathrm{S}} \hat{1}_{[0, R^{\mathrm{Y}}]}(r) J_0(\tilde{\mu}_m^{\mathrm{S}} r) \\ \bar{\lambda}_1^{\mathrm{S}} \tilde{R}_m^{(00)} \hat{1}_{[0, R^{\mathrm{Y}}]}(r) J_0(\tilde{\mu}_m^{\mathrm{Y}} r) & 0 \\ \bar{\lambda}_1^{\mathrm{S}} \tilde{R}_m^{(10)} \hat{1}_{[0, R^{\mathrm{Y}}]}(r) J_0(\tilde{\mu}_m^{\mathrm{Y}} r) & 0 \\ 0 & 0 \\ 0 & 0 \\ 0 & \bar{\lambda}_1^{\mathrm{C}} \tilde{R}_m^{(10)} \hat{1}_{[0, R^{\mathrm{Y}}]}(r) J_0(\tilde{\mu}_m^{\mathrm{Y}} r) \\ 0 & \bar{\lambda}_1^{\mathrm{C}} \tilde{R}_m^{(11)} \hat{1}_{[0, R^{\mathrm{Y}}]}(r) J_0(\tilde{\mu}_m^{\mathrm{Y}} r) \\ \bar{\lambda}_2^{\mathrm{C}} \tilde{R}_m^{\mathrm{C}} \hat{1}_{[0, R^{\mathrm{C}}]}(r) J_0(\tilde{\mu}_m^{\mathrm{C}} r) & \bar{\lambda}_2^{\mathrm{C}} \tilde{R}_m^{\mathrm{C}} \hat{1}_{[R^{\mathrm{Y}}, R^{\mathrm{C}}]}(r) J_0(\tilde{\mu}_m^{\mathrm{C}} r) \end{pmatrix};$$

$$\hat{1}_{[a,b]}(x) = \begin{cases} 1, & x \in [a,b], \\ 0, & x \notin [a,b]; \end{cases} \quad R_{\max} = \max\left(R^{\mathrm{C}}, R^{\mathrm{S}}\right);$$

$$\tilde{R}_m^{(00)} = \sum_s \frac{h_s^{\mathrm{Y}}(0) h_s^{\mathrm{Y}}(0)}{N_{ms}^{\mathrm{Y}}}; \quad \tilde{R}_m^{(01)} = \sum_s \frac{h_s^{\mathrm{Y}}(0) h_s^{\mathrm{Y}}(L^{\mathrm{Y}})}{N_{ms}^{\mathrm{Y}}};$$

$$\tilde{R}_m^{(10)} = \sum_s \frac{h_s^{\mathrm{Y}}(L^{\mathrm{Y}}) h_s^{\mathrm{Y}}(0)}{N_{ms}^{\mathrm{Y}}}; \quad \tilde{R}_m^{(11)} = \sum_s \frac{h_s^{\mathrm{Y}}(L^{\mathrm{Y}}) h_s^{\mathrm{Y}}(L^{\mathrm{Y}})}{N_{ms}^{\mathrm{Y}}};$$

$$\tilde{R}_m^{\mathrm{S}} = \sum_s \frac{h_s^{\mathrm{S}}(L^{\mathrm{S}}) h_s^{\mathrm{S}}(L^{\mathrm{S}})}{N_{ms}^{\mathrm{S}}}; \quad \tilde{R}_m^{\mathrm{C}} = \sum_s \frac{h_s^{\mathrm{C}}(0) h_s^{\mathrm{C}}(0)}{N_{ms}^{\mathrm{C}}}; \quad (15)$$

$$\tilde{Q}_m^{(0)} = F_m \sum_s \frac{h_s^{\mathrm{Y}}(0) G_s}{N_{ms}^{\mathrm{Y}}}; \quad \tilde{Q}_m^{(1)} = F_m \sum_s \frac{h_s^{\mathrm{Y}}(L^{\mathrm{Y}}) G_s}{N_{ms}^{\mathrm{Y}}}.$$

Equation (13) represents a matrix generalisation of the Fredholm integral equation of the second kind with the degenerate kernel, which, with the help of the standard substitution, is reduced to the linear algebraic system of equations [17] solved by using standard methods [18]. Thus, the temperature distribution in the active element and heatsinks can be found.

2.3 Numerical solution of the heat conduction problem

If the heat conductivity depends on temperature, equation (2) takes the from

$$\varkappa(T)\left(\frac{\partial^2 T}{\partial r^2} + \frac{1}{r}\frac{\partial T}{\partial r} + \frac{\partial^2 T}{\partial z^2}\right) + \frac{\partial \varkappa}{\partial T}\left[\left(\frac{\partial T}{\partial r}\right)^2 + \left(\frac{\partial T}{\partial z}\right)^2\right] + Q(r,z) = 0. \quad (16)$$

In this case, the problem was solved numerically. To obtain the difference schemes, we used the method of finite differences (which is simpler mathematically but leads to less specified schemes compared to variation–difference methods). Because the dimensions of the heatsinks significantly exceed (by 5–100 times in thickness) the dimensions of the active element, it is necessary to specify a nonuniform grid in the heatsinks, which has a small step near the Yb:YAG disk and increases away from it.

To solve the obtained algebraic system, we used the effective iteration schemes based on reducing the initial N-dimensional problem (in this case, two-dimensional) to a sequence of one-dimensional subproblems requiring the solution of linearised algebraic systems with three-diagonal matrices, which, in turn, can be solved by the sweep method. This scheme, called the method of alternating directions, is described, for example, in [19]. To solve the formulated problem, a small modification was required, which allowed one to obtain, for one dimensional subproblems, convergent systems of equations when homogeneous boundary conditions of the second kind are specified at both ends of the interval [expression (3) at $\gamma = 0$].

Compared to the simple iteration method and the Seidel method, which are the easiest for programming, this technique makes it possible to increase substantially the calculation speed. In the case of the model problem of the direct contact of the coolant with the active element, the calculation speed increases by 20 times; for the initial problem this increase is lower (two–three times) but it is still significant. This scheme differs from other effective schemes by a relative simplicity of programming and an efficient use of the specific matrix features of the linearlised system of the N-dimensional problem.

The comparison of the numerical solution and the solution obtained with the help of the method of Green's functions showed that they coincide fairly well in the case of the linear problem (the difference is no more than 1 %). The numerical solution requires more computer time but its algorithm is modified much simpler. The method of Green's functions does not allow one to take into account the temperature dependence of the heat conductivity but the solution obtained by this method in the linear approximation can be used as a seed value for a finite difference numerical scheme, which accelerates the calculation process.

2.4 Analysis of the solution of the heat conduction problem

In calculations we used the following parameters: the thickness of the Yb:YAG disk was 0.6 mm, its diameter – 10 mm, the atomic concentration – 10 %, and the orientation – [001]; the diameter of the copper heatsink was 70 mm, its thickness – 60 mm; the diameter of the sapphire disk was 30 mm and its thickness – 3 mm. The diameter of the pump beam was 6 mm. The heat release power

$$P_{\mathrm{heat}} = Q_0 \int_0^{R^{\mathrm{Y}}} f(r) r \mathrm{d}r \int_0^{L^{\mathrm{Y}}} g(z) \mathrm{d}z \quad (17)$$

was ~ 100 W (~ 350 W cm^{-2} per unit cross section of the beam).

Figure 2 demonstrates the dependences of the temperatures maximum and average in the beam region on P_{heat} upon cooling by one (copper) and two (copper and sapphire) heatsinks. This figure also shows the dependences corresponding to the intermediate regime at which the sapphire disk is not in contact with the coolant. In this

case, the gain in the temperature with respect to the scheme with one heatsink is explained by the fact that a part of heat released by the active element to sapphire spreads along the radius in it and is transferred via the active element to the copper heatsink outside the beam region. This regime is less efficient than that with two heatsinks but does not require additional efforts to provide heat removal from the sapphire.

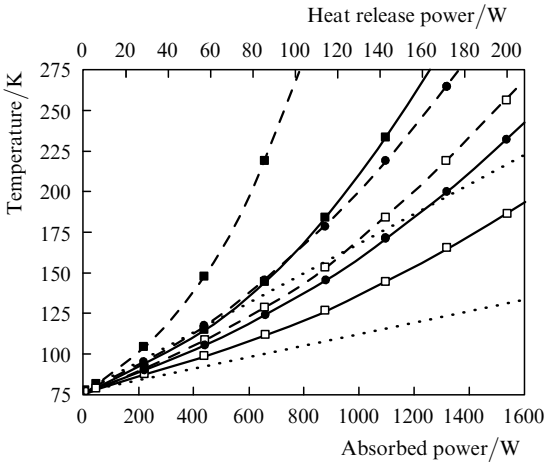

Figure 2. Dependences of the maximal (dashed curves) Yb : YAG temperature and the Yb : YAG temperature averaged over the beam region (solid curves) on the heat release power and absorbed pump radiation power upon cooling by one copper heatsink (■), a copper heatsink and a sapphire disk (●), and two heatsinks (□). Dotted lines are the linear approximation of the top and bottom curves. The coolant temperature is 77 K.

At the heat power $P_{\text{heat}} = 100$ W, the nonlinear effects substantially influence the solution because the heat conductivity of YAG decreases two-fold when the temperature changes from 77 K to 107 K [6]. Thus, when the active element is cooled only from one end, the maximum temperature in the crystal exceeds 150 K already at $P_{\text{heat}} = 60$ W. The use of the second heatsink makes it possible to increase the power up to 110 W at the same maximum temperature and at $P_{\text{heat}} = 100$ W, the temperature does not exceed 140 K.

Thus, for the amplifier parameters under consideration, the temperature of the active element can be restrained within 150 K at $P_{\text{heat}} \sim 100$ W.

3. Solution of the elasticity problem

In the linear approximation (Hooke law) the tensor of elastic stresses $\hat{\sigma}$ is related to the strain tensor $\hat{u}$ and temperature T by the expression

$$\sigma_{ij} = \lambda_{ijkl}\left[u_{kl} - \int_{T_0}^{T} \alpha_{kl}(T')\mathrm{d}T'\right], \tag{18}$$

where $\hat{\lambda}$ is the elastic stiffness tensor; $\hat{\alpha}$ is the thermal expansion tensor; T_0 is the initial temperature at which the body in the absence of stresses is assumed unstrained. Hereafter, we imply summation in the recurrent indices from 1 to 3 and the subscripts i, j also take values from 1 to 3 [8].

When the external volume forces are neglected, the conditions for the equilibrium of the strained body in the internal region have the from

$$\frac{\partial \sigma_{ij}}{\partial x_j} = 0\,, \tag{19}$$

the conditions on the free boundary imply the equality to zero of normal and shear stresses on the sample surface [20]:

$$\sigma_{ij} n_j|_{\Gamma} = 0, \tag{20}$$

where Γ is the body surface; n_j are the vector components of the external normal to it.

The YAG crystal is cubic but we will assume it to be isotropic. This simplifying assumption allows us to reduce the problem to two coordinate one in the coordinate system r, z. In this case, at small deformations the tensor $\hat{u}$ has the following nonzero components [20]:

$$u_{rr} = \frac{\partial U_r}{\partial r},\ u_{\phi\phi} = \frac{U_r}{r},\ u_{zz} = \frac{\partial U_z}{\partial z},\ u_{rz} = \frac{1}{2}\left(\frac{\partial U_r}{\partial z} + \frac{\partial U_z}{\partial r}\right), \tag{21}$$

where U_r and U_z are the components of the shear vector; ϕ is the polar angle. The system of equations (18)–(21) represents a closed boundary problem for these components.

The temperature dependence of the thermal expansion coefficient is presented in [6]. The author of paper [6] speaks about a weak temperature dependence of the tensor components of the elastic stiffness (the difference in the components at $T = 100$ K and 300 K is no more than 10 %), which we will neglect.

To solve the elasticity problem, a finite element numerical code was written. The solution was found by using the method of alternating directions discussed above. The order of approximation of differential operators by difference operators was equal to 2 on the entire grid.

At $P_{\text{heat}} = 100$ W in the case of cooling by two heatsinks, the components of the deformation tensor do not exceed 3.2×10^{-4} in the absolute value, which confirms the applicability of the Hooke law and expressions (21), and the elastic stresses in the crystal do not exceed 3.4×10^7 Pa, which is six times lower than the maximum admissible values for the undoped YAG [2].

4. Calculation of thermally induced beam distortions

When calculating the thermally induced beam distortions, we took into account the change in the shape of the active element (together with the dielectric mirror coated on it), the temperature dependence of the refractive index, the electronic change in the refractive index (the change in the refractive index as a function of the populations of the of active ion levels) [21], and the photoelastic effect. The expression

$$\delta L_m = \left\{(n_0 - 1)u_{zz} + [n(T) - n_0] + \frac{2\pi}{9n_0}(n_0^2 + 2)^2 \Delta p \Delta N - \frac{n_0^3}{2}\Delta B_{mm}\right\}\mathrm{d}z \tag{22}$$

can be written for a change in the optical length upon the beam propagation through the element dz. Here $n_0 = n(T_0)$ is the unperturbed refractive index; Δp is the difference in polarisations of the Yb^{3+} ion in the ground state and at the upper working level; ΔN in the case of the operation in accordance with the four-level scheme is equal to the difference in populations of working laser levels; $\Delta\hat{B}$ is the change in the dielectric impermeability tensor*, caused by the photoelastic effect:

$$\Delta B_{ij} = \pi_{ijkl}\sigma_{kl}; \tag{23}$$

$\hat{\pi}$ is the tensor of piezooptic coefficients. Expression (22) is valid for radiation polarised along two mutually perpendicular axes $m = \mu$ and v for which $\Delta B_{\mu v} = 0$. These directions at each point of the crystal are different in the general case. We neglected the deviation of the beam rays from direct ones, parallel to the z axis. The four terms in braces describe the change in the element length, temperature and electronic changes in the refractive index, and the photoelastic effect, respectively.

If intrinsic polarisations (along the axes μ and v) are independent of z, by integrating (22) in z we obtain the change in the optical length of the path per two passes of radiation (with relection from the mirror). In the general case, to take into account the anisotropy caused by the photoelastic effect, we will use the formalism of Jones matrices [22].

We introduce the Cartesian coordinates x, y in the plane of the beam cross section. Let radiation incident on the active disk be linearly polarised along the x axis (x_0 and y_0 are the unit vectors of x and y axes, respectively). The polarisation vector $\boldsymbol{\xi}$ of the field at the crystal output (after two passes) can be found by multiplying the Jones matrices for the elements of the medium with centres in the grid nodes used for the finite element approximation of the elasticity problem. In the Jones matrices we took into account only the phase difference of intrinsic polarisations, while the average phase was calculated separately. In this case, the expression for $\boldsymbol{\xi}$ contains also, apart from information on polarisation, the astigmatic component of the phase. Then, the expression for the phase incursion of the propagated wave component, which is polarised long the x axis, has the from

$$\Delta\varphi(x,y) = 2k_0\left\{[-(n_0-1)U_z|_{z=0} + n_0 U_z|_{z=L^Y}] + \int_0^{L^Y}[n(T)-n_0]\mathrm{d}z + \frac{2\pi}{9n_0}(n_0^2+2)^2\Delta p\int_0^{L^Y}\Delta N\mathrm{d}z - \frac{n_0^3}{2}\int_0^{L^Y}\frac{\Delta B_{xx}+\Delta B_{yy}}{2}\,\mathrm{d}z\right\} + \arctan\frac{\mathrm{Im}(\boldsymbol{\xi}\boldsymbol{x}_0)}{\mathrm{Re}(\boldsymbol{\xi}\boldsymbol{x}_0)}, \tag{24}$$

where k_0 is the wave number in the free space. Expression (24) allows one to calculate the focal distance of the thermally induced lens and its aberrations. The local (Γ_d) and integral (γ_d) depolarisation rates for the nongyrotropic medium are expressed as

$$\Gamma_\mathrm{d}(x,y) = |\boldsymbol{\xi}\boldsymbol{y}_0|^2, \quad \gamma_\mathrm{d} = \frac{\iint\Gamma_\mathrm{d}|\boldsymbol{E}_\mathrm{in}|^2\mathrm{d}x\mathrm{d}y}{\iint|\boldsymbol{E}_\mathrm{in}|^2\mathrm{d}x\mathrm{d}y}, \tag{25}$$

where E_in is the field intensity of incident radiation; integration is performed over the beam cross section.

It is easy to show that for radiation polarised along the y axis, the depolarisation rate will be the same, and the expression for the phase incursion will differ from (24) by the sign in front of the last term. By using the produced numerical code, the depolarisation degree and the phase incursion were calculated for a crystal with an arbitrary orientation of crystallophysic axes. The method implied is described in [3, 23].

Figure 3 presents stigmatic and astigmatic components of the phase incursion and the profile of the depolarisation rate of the beam, which were calculated for a crystal with the [001] orientation in the minimum of the integral depolarisation rate (input radiation is linearly polarised at the angle 45° to the crystallophysic axis) at $P_\mathrm{heat} = 100$ W in the case of cooling the active element by two heatsinks. The temperature dependence $n(T)$ for YAG was borrowed from [6] and the value of Δp – from [21]. We also took into account the contribution to the formation of the thermal lens caused by the $n(T)$ dependence for the sapphire.

In Fig. 3, the negative phase corresponds to the positive lens and vice versa. The main contribution to the formation of the thermally induced lens is made by the curvature of the mirror coated on the crystal surface. This convex mirror produces the resultant negative lens, although the term in (22) responsible for the temperature change in the refractive index makes a positive contribution. The contribution of the photoelastic effect is positive in the polarisation plane and negative in the plane perpendicular to it.

The beam distortions at $P_\mathrm{heat} = 100$ W are small: the focal distance of the thermally induced lens is less than 5.5 m in the beam region in the absolute value; the maximum values of Γ_d lie outside the beam region and the integral depolarisation rate is $\gamma_\mathrm{d} = 3.8\times10^{-4}$.

The mirror becomes significantly convex (the displacement of its surface along the z axis can be up to 1 μm) and, hence, the loss of the thermal contact with the copper heatsink is possible in the beam region, which will result in an additional increase in the temperature. This fact should be taken into account in performing experiments.

5. Conclusions

Taking into account the temperature dependences of the medium parameters, we have calculated the thermally induced beam distortions in a disk Yb : YAG laser amplifier with a high average power in the stationary regime. We have shown that the use of cryogenic cooling makes it possible to obtain high-quality output radiation at thermal loads ~ 350 W cm^{-2}. If the heat release power is 13 % of the absorbed radiation power and the conversion efficiency of the stored energy into the energy of output radiation is approximately 70 %, the increment of the laser radiation intensity at the output of one amplifier will be $\sim$1750 W cm^{-2}.

The increase in the power is restricted by the heat conductivity of the active element, which rapidly decreases with increasing temperature, but the increase in the thermal load by 1.5–2 times, when the dimensions of the active element remain invariable, is admissible. On this basis the

* The dielectric impermeability tensor is a tensor inverse to the dielectric constant tensor.

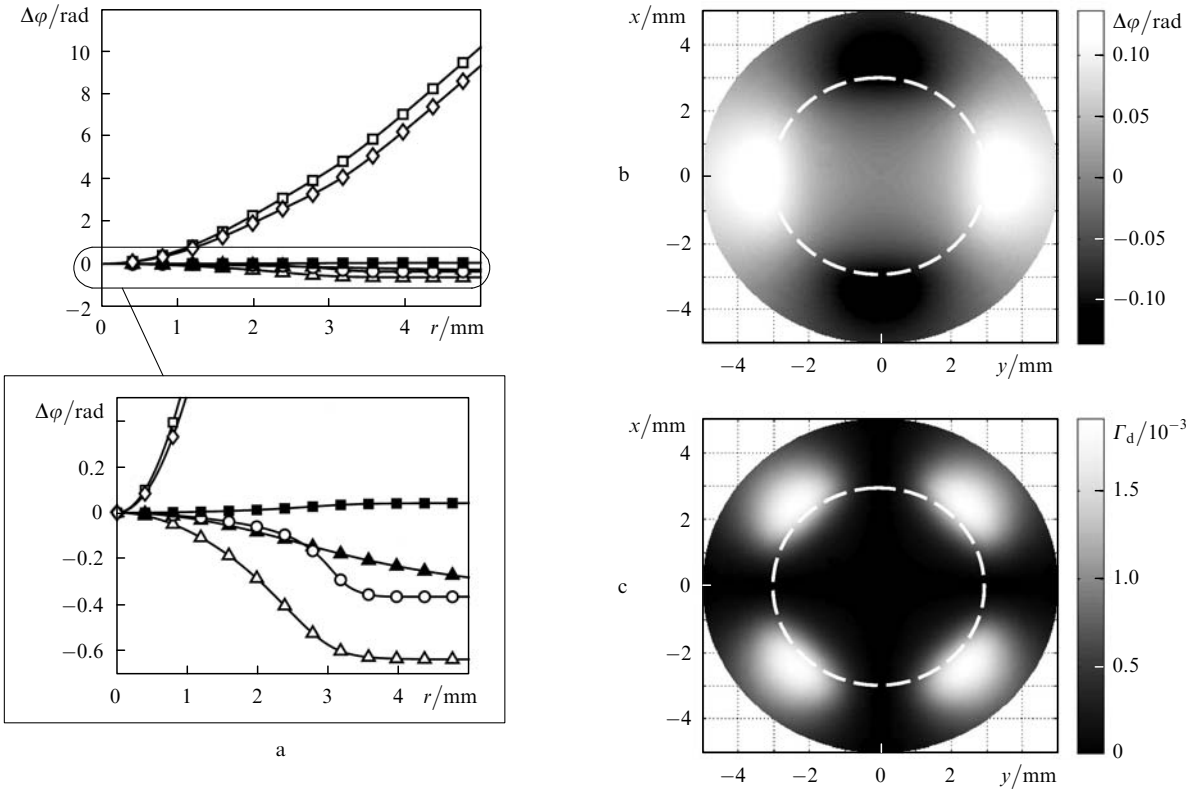

Figure 3. Thermally induced distortions of the laser beam per two passes through the amplifier: the stigmatic component of the phase incursion (◇), including geometrical distortion (□), temperature variations of the refractive index in Yb : YAG (△) and sapphire (▲), electronic change in the refractive index in Yb : YAG (○), and photoelastic distortions (■) (a) as well as the astigmatic component of the phase incursion (b) and the local rate of depolarisation (c). In Figs 3b and c radiation is polarised long the x axis and white dashed circles show the regions of the pump beam.

use of active media with small thermal losses makes it possible to design compact lasers with the average power of ~ 1 kW.

At present, experiments on studying amplification in cryogenic Yb disks for the pump power up to 600 W (the beam diameter is 3 mm and the power density is 6.1 kW cm^{-2}) are being performed at the Institute of Applied Physics, RAS. The experimental results achieved in [24] well agree with the presented calculations.

Acknowledgements. This work was supported by the program of the Presidium of the Russian Academy of Sciences 'Femtosecond Optics and New Optical Materials' and the Russian Foundation for Basic Research (Grant No. 08-02-99044-r_ofi).

References

1. Mezenov A.V., Soms L.N., Stepanov A.I. *Termooptika tverdotel'nykh lazerov* (Thermal Optics of Solid-State Lasers) (Leningrad: Mashinostroenie, 1986) p. 199.
2. Koechner W. *Solid-state Laser Engineering* (Berlin: Springer-Verlag, 1999).
3. Khazanov E.A. *Opt. Lett.*, **27**, 716 (2002).
4. Soloviev A.A., Snetkov I.L., Zelenogorsky V.V., Kozhevatov I.E., Palashov O.V., Khazanov E.A. *Opt. Express*, **16**, 21012 (2008).
5. Brown D.C. *IEEE J. Sel. Top. Quantum Electron.*, **11**, 587 (2005).
6. Brown D.C. *IEEE J. Quantum Electron.*, **33**, 861 (1997).
7. Tidwell S.C., Seamans J.F., Bowers M.S., Cousins A.K. *IEEE J. Quantum Electron.*, **28**, 997 (1992).
8. Nye J. *Physical Properties of Crystals: Their Representation by Tensors and Matrices* (London: Oxford Univ. Press, 1987; Moscow: Mir, 1976).
9. Brown D.C. *IEEE J. Quantum Electron.*, **34**, 560 (1998).
10. Fan T.Y. *IEEE J. Quantum Electron.*, **29**, 1457 (1993).
11. Contag K., Karszewski M., Stewen C., Giesen A., Hugel H. *Kvantovaya Elektron.*, **28**, 139 (1999) [*Quantum Electron.*, **29**, 697 (1999)].
12. Tokita S., Kawanaka J., Fujita M., Kawashima T., Isawa Y. *Appl. Phys. B*, **80**, 635 (2005).
13. Patel F.D., Honea E.C., Speth J., Payne S.A., Hutcheson R., Equall R. *IEEE J. Quantum Electron.*, **37**, 135 (2001).
14. Chénais S., Forget S., Druon F., Balembois F., Georges P. *Appl. Phys. B*, **79**, 221 (2004).
15. Polyanin A.D. *Spravochnik po lineinym uravneniyam matematicheskoi fiziki* (Handbook on Linear Equations of Mathematical Physics) (Moscow: Fizmatlit, 2001).
16. Hemming R.W. *Digital Filters* (Englewood Cliffs: Prentice-Hall, 1977; Moscow: Sov. radio, 1980).
17. Sobolev S.L. *Uravneniya matematicheskoi fiziki* (Equations of Mathematical Physics) (Moscow: Nauka, 1966).
18. Berezin I.S., Zhidkov N.P. *Metody vychislenii* (Calculation Methods) (Moscow: Fizmatlit, 1959) Vol. II.
19. Samarskii A.A. *Teoriya raznostnykh skhem* (Theory of Finite-Difference Schemes) (Moscow: Nauka, 1977).
20. Landau L.D., Lifshits E.M. *Theory of Elasticity* (Oxford: Pergamon Press, 1970; Moscow: Nauka, 1987).
21. Antipov O.L., Bredikhin D.V., Eremeikin O.N., Ivakin E.V., Savikin A.P., Sukhodolov A.V., Fedorova K.A. *Kvantovaya Elektron.*, **36**, 418 (2006) [*Quantum Electron.*, **36**, 418 (2006)].
22. Jones R.C. *J. Opt. Soc. Am.*, **31**, 488 (1941).
23. Koechner W., Rice D.K. *J. Opt. Soc. Am.*, **61**, 758 (1971).
24. Perevezentsev E.A., Mukhin I.B., Palashov O.V., Khazanov E.A. *Kvantovaya Elektron.*, **39**, 807 (2009) [*Quantum Electron.*, **39**, 807 (2009)].